Applied Catalysis B: Environmental 305 (2022) 121064

Contents lists available at ScienceDirect

Applied Catalysis B: Environmental

journal homepage: www.elsevier.com/locate/apcatb

Surface molecule induced effective light absorption and charge transfer for H_2 production photocatalysis in a carbonized polymer dots-carbon nitride system

Mei Han [a,1], Chunyuan Kang [a,1], Zexing Qu [a,b,*], Shoujun Zhu [a,c], Bai Yang [a,c,*]

[a] State Key Laboratory of Supramolecular Structure and Materials, College of Chemistry, Jilin University, Changchun 130012, PR China
[b] Institute of Theoretical Chemistry and Laboratory of Theoretical & Computational Chemistry, Jilin University, Changchun 130023, PR China
[c] Joint Laboratory of Opto-Functional Theranostics in Medicine and Chemistry, The First Hospital of Jilin University, Changchun 130021, PR China

ARTICLE INFO

Keywords:
Carbonized polymer dots
Density functional theory
Photocatalytic hydrogen production
Charge transfer

ABSTRACT

Current sunlight-powered H_2 production that employ carbonized polymer dots (CPDs)-graphitic carbon nitride (g-C_3N_4) systems has made significant progress. However, we still have a limited understanding of the mechanism by which CPDs contribute to the phtocatalytic efficiency. Surface molecule 1,2,3,5-tetrahydro-5-oxo-imidazo[1,2-α]pyridine-7-carboxylic acid (IPCA) has been verified to largely impact the photophysical properties of CPDs. Here, we report the design of g-C_3N_4, IPCA-g-C_3N_4 and CPDs-g-C_3N_4 catalysts to uncover the critical role of IPCA. The photocatalytic H_2 production rates of g-C_3N_4 were improved by the hybridization with IPCA and CPDs (1172 ± 39; 2150 ± 92 vs. 828 ± 121 μmol g^{-1} h^{-1}, respectively). The DFT calculations further unraveled that electron transfer pathway in ICPA-CN@H_3O^+ followed ICPA -> g-C_3N_4 -> H_3O^+ procedure. The results indicate that IPCA on CPDs is conducive to extending the light-responsive range, redistributing of photoinduced electron-hole pairs, increasing the electron density of g-C_3N_4, and thus improving H_2 generation rates.

1. Introduction

Driven by the prospect of addressing both worldwide energy shortage and environmental contamination issues, the exploitation of clean and renewable energy is attracting enormous interests [1,2]. Hydrogen (H_2) is an ultimate clean and sustainable energy source, allowing for an energy cycle free of greenhouse gas. Thus, H_2 is regarded as an ideal replacement for depleting fossil fuel reserves. Much attention has been paid to the research of H_2 [3–5]. Production of H_2 from water splitting using inexhaustible solar energy is one of the most promising solutions to the growing demand for energy and associated environmental concerns [6,7]. Tremendous efforts have been dedicated to photocatalytic H_2 production, surely making significant achievements over the past few years [8–10]. Bearing the above in mind, it is suggested that the photocatalyst holds the key to the photocatalytic reactions. Thus, seeking low-cost and environmentally benign photocatalysts with sufficiently high activity and stability remains the core challenge [11].

Carbon dots (CDs) are increasingly explored as novel nanomaterials for their promising applications in the fields of optoelectronic devices [12], bio-imaging [13], catalysis [14–16], etc. A new classification of CDs, named carbonized polymer dots (CPDs) is revealed as an emerging class of CDs with distinctive polymer/carbon hybrid structures and properties [17–19]. Due to the electron-withdrawing and -donating properties, CPDs are further proved to be the co-catalytic active site to improve photocatalytic activity [20]. Graphitic carbon nitride (g-C_3N_4) with a poly-(tri-s-triazine) (polyheptazine) building block (often referred as melon) has recently emerged as an attractive visible-light absorber and can generate H_2 photocatalytically [21–24]. Given the poor light-harvesting performance and catalytic activity, lots of skilled incorporation techniques have been developed for manufacturing efficient composites [25,26]. The suitable structure and ultrahigh stability make g-C_3N_4 an ideal host for robustly accommodating CPDs [27].

Much less is known on the precise structure or co-catalytic mechanism of CPDs as researchers primarily focus on the graphitic sp^2 carbonaceous cores [28,29]. Recently, Yang's group have investigated the photoluminescent mechanism of CPDs which were prepared using citric acid and ethylenediamine as precursors, and identified the molecular emssion center of a citrazinic acid derivative 1,2,3,

* Corresponding authors at: State Key Laboratory of Supramolecular Structure and Materials, College of Chemistry, Jilin University, Changchun 130012, PR China.
E-mail addresses: zxqu@jlu.edu.cn (Z. Qu), byangchem@jlu.edu.cn (B. Yang).
[1] These authors contributed equally: Mei Han, Chunyuan Kang.

https://doi.org/10.1016/j.apcatb.2022.121064
Received 28 September 2021; Received in revised form 14 December 2021; Accepted 2 January 2022
Available online 4 January 2022

5-tetrahydro-5-oxo-imidazo[1,2-α]pyridine-7-carboxylic acid (denoted as IPCA) [30]. The optical properties of CPDs are strongly dependent on the covalently-bound/encapsulated IPCA and its analogs [30–33]. And the surface molecule IPCA also acts as the isolated conjugating units to provide CPDs with new energy levels [34]. It is fundamental to understand the essence of surface-functional-molecule, which contributes to smart design of high-performance photocatalyst.

In this study, we report the design and synthesis of g-C_3N_4, IPCA-g-C_3N_4 (IPCA-CN) and CPDs-g-C_3N_4 (CPDs-CN) catalysts (Scheme 1). The aim of this work is to identify the crucial roles of surface molecule IPCA, commonly observed in CPDs from the pyrolysis citric acid and amines, in enhancing photocatalytic performance in a CPDs-CN system. Upon the hybridization of IPCA and CPDs, improved photocatalytic H_2 production activity of g-C_3N_4 were observed (1172 ± 39; 2150 ± 92 vs. 828 ± 121 μmol g^{-1} h^{-1}, respectively). We further employed theoretical calculations based on density functional theory (DFT) to elucidate the underlying mechanism of the catalytic efficiency improvement.

2. Experimental section

2.1. Reagents

All reagents were obtained from commercial suppliers and used without further purification. Citric acid (CA) was purchased from Aladdin. Ethylenediamine (EDA) was purchased from Alfa Aesar. Dicyandiamide (DCD) was purchased from Aladdin Industrial Corporation. Selenium (Se) was purchased from Shanghai Macklin Biochemical Co., Ltd. Na_2SO_4 was obtained from Sinopharm Chemical Regent. Chloroplatinic acid ($H_2PtCl_6{\cdot}6H_2O$) was purchased from Energy Chemical. Deionized (DI) water (> 18 MΩ cm) were generated via a Milli-Q system. Other organic solvents were purchased from Beijing Chemical Works.

2.2. Synthesis

2.2.1. Synthesis of CPDs

CPDs was synthesized via a modified method according to our previous work with some modifications [35]. Briefly, 192 mg of CA (1.0 mmol) and 67 μL of EDA (1.0 mmol) were dissolved in 10 mL of deionized water. Then, the solution was transferred to a poly (tetrafluoroethylene) (Teflon)-lined autoclave (25 mL) and heated at 200°C for 6 h. After cooling down, the product was subjected to dialysis with molecular weight cut off 500–1000. The brown powder CPDs was finally obtained by freeze-drying.

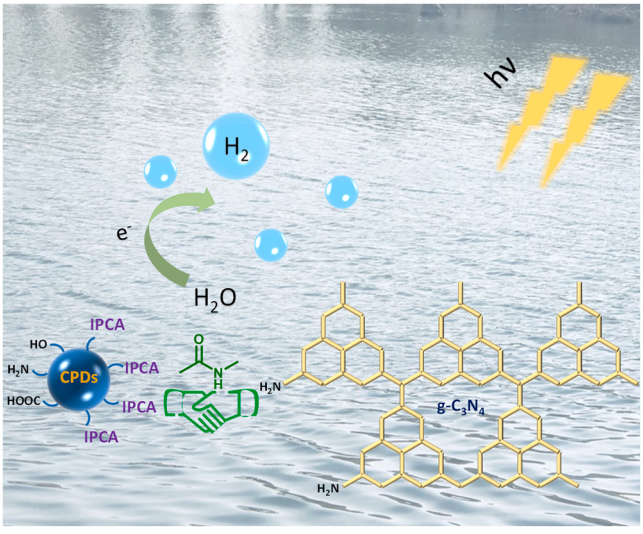

Scheme 1. Schematic illustration for the design and synthesis of composite photocatalyst and the photocatalytic water splitting for H_2 production.

2.2.2. Synthesis of IPCA

IPCA was synthesized by the hydrothermal method and purified by column chromatography in accordance with previously published work [30]. Methanol/ethyl acetate (2:1) was selected as the eluent.

2.2.3. Synthesis of CPDs-CN-x

The synthetic procedure was based on previous work [36]. Typically, the mixture of 10 g DCD and 1 g Se powder were dispersed in 50 mL ethanol, stirred for 1 h at room temperature, and dried at 60°C oven. Then, the mixture was annealed at 650 °C for 3 h in static air atmosphere in a muffle furnace. Thereafter, 100 mg of the powder was added to x mL (x = 3 or 7) of CPDs solution (1 mg mL^{-1}) and water was added to a total volume of 10 mL. Subsequently, the mixture was transferred to a Teflon-lined autoclave (25 mL) and heated at 180 °C for 6 h. After the reaction, the reactors were cooled to room temperature naturally. The product was centrifuged and washed with DI water for three times and dried at 60 °C oven. The final products were obtained and donated as CPDs-CN-x, where x denotes the amount of CPDs relative to that of g-C_3N_4 [x (wt%) = CPDs/g-C_3N_4 × 100]. CPDs-CN-7 was referred as CPDs-CN unless otherwise stated.

2.2.4. Synthesis of IPCA-CN

The synthetic procedure was similar to that of CPDs-CN, except that CPDs was replaced with IPCA solution (2 mL, 1 mg mL^{-1}).

2.2.5. Synthesis of g-C_3N_4

The synthetic procedure was similar to that of CPDs-CN, except that CPDs was replaced 10 mL of DI water.

2.3. Characterization

The ultraviolet-visible (UV–vis) absorption spectra were obtained using a Shimadzu 3100 UV–vis spectrophotometer. The UV–vis DRS spectra were acquired on a UV/VIS/NIR spectrophotometer (Lambda 950, Perkinelmer). And the absorption spectra were calculated from the reflectance data with the Kubelka-Munk function. Transmission electron microscopy (TEM) were performed on a JEM-2100 F at an accelerating voltage of 200 kV. ^{1}H NMR and ^{13}C NMR spectra were performed with AS 400 (Q.One Instruments Ltd., 400 MHz). X-ray diffraction (XRD) patterns were conducted with Cu Kα radiation (λ = 1.5406 Å) operating at 40 kV and 40 mA with a fixed slit (PANalytical B.V. Empyrean). Steady-state fluorescence spectra and fluorescence decay curves were collected on FLS 920 (Edinburgh Instrument). The XPS spectra were conducted on Thermo ESCALAB-250Xi spectrometer with a mono X-ray source with Al Kα excitation. Synchronous illumination X-ray photoelectron spectroscopy (SIXPS) characterization was used to investigate the electron density changes on prepared samples under irradiation using R3000/VUV5K/MX-650 (PREVAC, Poland) system. In the process of measurements, the changes of XPS spectra were recorded by controlling light on or off. A 300 W xenon lamp (CEL-HXF300, Beijing Ceaulight Technology Co., Ltd., China) was equipped with an air mass 1.5 global (AM 1.5G, 100 mW cm^{-2}) filter or a 420 nm cutoff filter.

2.4. Electrochemical characterization

Electrochemical impedance spectroscopy (EIS) and transient photocurrent response measurements were carried out in a conventional three electrode cell (CH Instruments, Chenhua, Shanghai, China). The working electrodes were prepared as follows: the photocatalyst (2 mg mL^{-1}) was dispersed in ethanol and then spin-coated onto FTO glass (1 × 1 cm^{-2}). After air-drying for 2 h, the working electrode was further dried in the oven at 60 °C to improve adhesion. Pt-electrode was employed as counter electrode. Ag/AgCl electrode was used as reference electrode. EIS experiments were performed within a frequency range

from 10^{-1} Hz to 2×10^5 Hz. The photocurrent-time dependence was measured under chopped irradiation with 30 s light on/off cycles. Na_2SO_4 solution (0.1 M) was used as the electrolyte in the electrochemical experiments.

2.5. Photocatalytic reaction

The photocatalytic experiments were prepared in reaction cell by first dispersing the as-prepared catalysts (20 mg) in aqueous TEOA solutions (10 vol%, 5 mL) by sonication treatment. Prior to illumination, the reactor is deaerated by evacuation to assure vacuum environment with stirring for 20 min. And then the suspension was irradiated from the top of the reaction cell through a quartz window a 300 W xenon lamp. During irradiation, the temperature was maintained at 6 °C by a flow of cooling water and the samples were constantly stirred. The amount of generated H_2 was analyzed using an online gas chromatograph (GC-7920, high purity N_2 as carrier gas) every half an hour. Thermal conductivity detection (TCD) was used to quantify H_2 productions in the headspace during photocatalysis. Pt-cocatalyst was synthesized via in situ photo-deposition by adding a unique amount of $H_2PtCl_6 \cdot 6H_2O$ aqueous solution as a precursor and the deposition amount of metallic Pt was 2 wt%.

2.6. Apparent quantum yield determination

The wavelength-dependent apparent quantum yield (AQY) was measured with a similar device. The difference was that AM 1.5G filter was replaced with the corresponding monochromatic-light filters. The irradiation area was ~ 12.56 cm^2. The total intensity of irradiation was measured by an irradiation meter (CEL-FZ-A). The evolved headspace gas was analyzed by gas chromatography and the AQY (%) calculated via Eq. (1):

$$AQY(\%) = 100 \times \frac{2n_{H2}NAhc}{tirr\lambda IA} \quad (1)$$

Where n_{H2} is the moles of H_2 generated, N_A Avogadro's constant (6.02×10^{23} mol^{-1}), h is the Planck constant (6.63×10^{-34} J s), c is the speed of light (3×10^8 m s^{-1}), t_{irr} the irradiation time (s), λ the wavelength of incident monochromatic light (m), I the light intensity (W m^{-2}) and A the cross-sectional area of irradiation (m^2).

2.7. Computational details

In this work, we use IPCA as the model of CPDs and g-C_3N_4 is used to mimic the graphitic carbon nitride (g-C_3N_4). The details for the structures could be found in Fig. 1a. All the calculations were performed using the density functional theory (DFT) within Gaussian 16 package [37]. The equilibrium geometries of g-C_3N_4 and IPCA-CN were optimized using the B3LYP functional [38,39] and the 6–31 G(d) basis set [40]. For the calculations on g-C_3N_4@H_3O^+ and IPCA-CN@H_3O^+ complexes, different binding site of H_3O^+ interacting with g-C_3N_4 and ICPA-CN were compared and the best site was found at the top region of g-C_3N_4 above C atom. The UV–vis absorption spectrum and the excited state calculations were performed using TDDFT with the optimized geometries at B3LYP/6-31G(d) level.

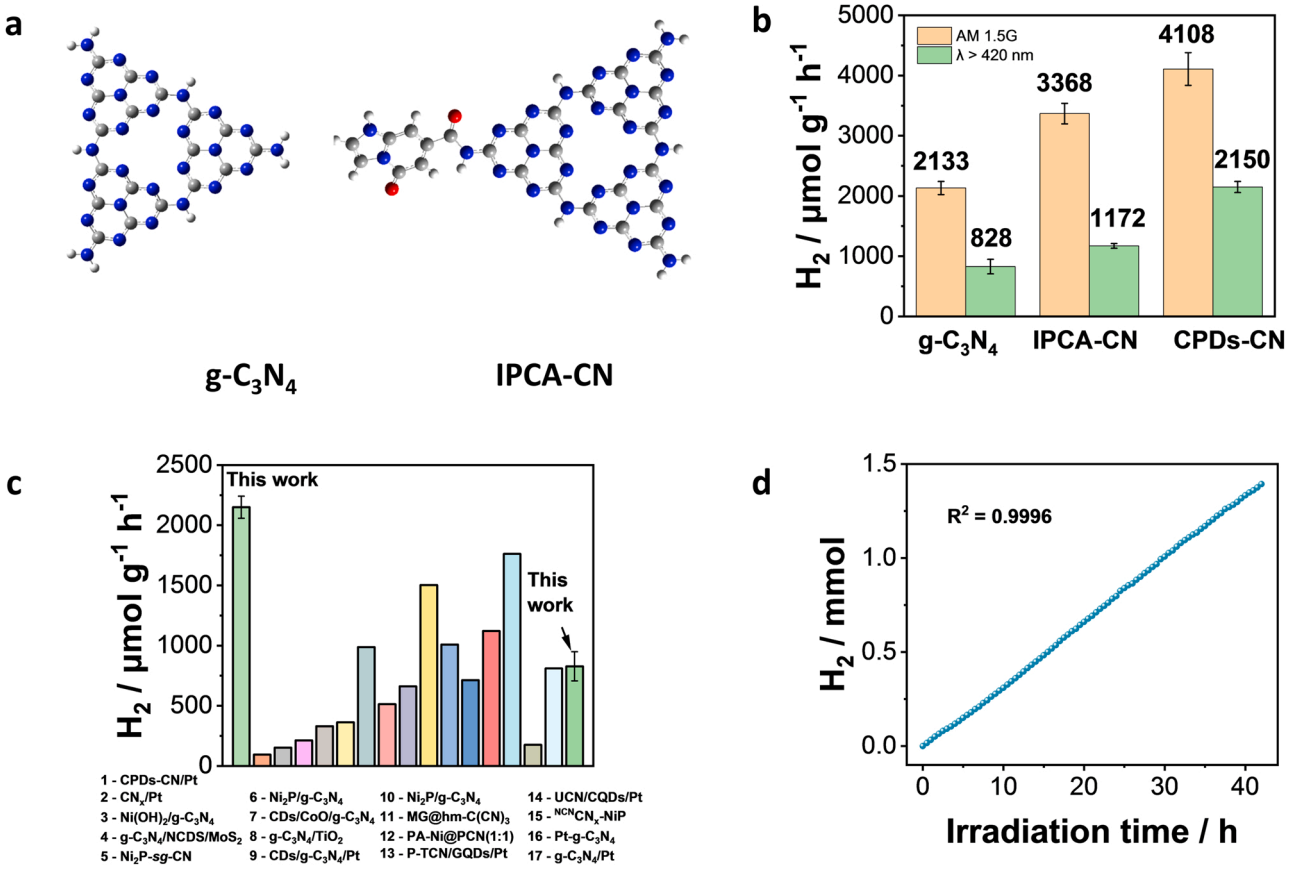

Fig. 1. a) The structure models of g-C_3N_4 and IPCA-CN. Color code: grey C; blue N; white H; red O. b) Photocatalytic H_2 production rates from water splitting. c) Comparison of the photocatalytic activities of catalysts for H_2 generation reported in the literatures; details as the Table S1. d) Long term photocatalytic performance towards H_2 evolution over CPDs-CN catalyst under visible light irradiation (42 h, $\lambda > 420$ nm, 6 °C).

3. Results and discussion

3.1. Photocatalytic properties

The photocatalytic H_2 generation systems were assembled in a photoreactor by dispersing catalyst powders in an aqueous solution of the sacrificial electron donor triethanolamine (TEOA). The results were summarized in Fig. 1b. g-C_3N_4 generated H_2 with a production rate of 2133 ± 109 μmol g^{-1} h^{-1} under simulated sunlight irradiation. The increase in photocatalytic H_2 production rate was observed to be 3368 ± 171 μmol g^{-1} h^{-1} on IPCA-CN. CPDs-CN had the H_2 production rate of 4108 ± 271 μmol g^{-1} h^{-1}. Under visible irradiation ($\lambda > 420$ nm), the photocatalytic H_2 evolution rates reached 828 ± 121, 1172 ± 39 and 2150 ± 92 μmol g^{-1} h^{-1}, respectively. Notably, photo-H_2 generation with CPDs-CN catalyst was also proved to be significantly higher than that previously reported with g-C_3N_4-composite systems (Fig. 1c and Table S1). The AQY was measured to evaluate the light utilization efficiency for H_2 evolution under the illumination of monochromatic light. In Fig. S1, AQY decreased with increasing wavelength, which achieved 2.5% at 420 nm and 0.22% at 500 nm. Fig. 1d illustrates the H_2 evolution from long-term (42 h) photocatalytic reaction containing the CPDs-CN catalysts. The H_2 evolution remained stable at an approximate rate of 33.9 μmol h^{-1} for 42 h without a rate decay ($R^2 = 0.9996$). The result identified the stability of the material, which contributed to the stable transport of photogenerated electrons.

Indeed, semiconductor g-C_3N_4 possess the characteristics of outstanding stability resistant to photo-induced decomposition in aqueous system. After 12 h of illumination in aqueous system, no liquid products were detected according to ^{1}H NMR spectra (Fig. 2a). Furthermore, XRD results in Fig. 2b showed that the two characteristic diffraction peaks at 13.0° and 27.8° attributed to the (100) crystal plane of the in-plane repeating tri-s-thiazine units and the (002) crystal plane of the stacking of the conjugated aromatic structure, respectively, were detected, signifying structural stability of CPDs-CN catalyst in aqueous system under irradiation.

3.2. Characterization of the photocatalysts

It was revealed that loading of CPDs on g-C_3N_4 can largely increase the catalytic performance. The remarkable features of CPDs promote us to elucidate better understanding of the complex. A series of experiments were carried out. Primarily, CPDs were designed and synthesized using multifunctional molecules citric acid (CA) and ethylenediamine (EDA) as precursors [35]. Polymer clusters were first formed due to the condensation and crosslinking [41]. Through further dehydration and carbonization, polymer/carbon hybrid structure of CPDs was formed [17,42]. Transmission electron microscopy (TEM) images show that CPDs are graphitic with average diameters of 1.9 nm (Fig. S2). Lattice

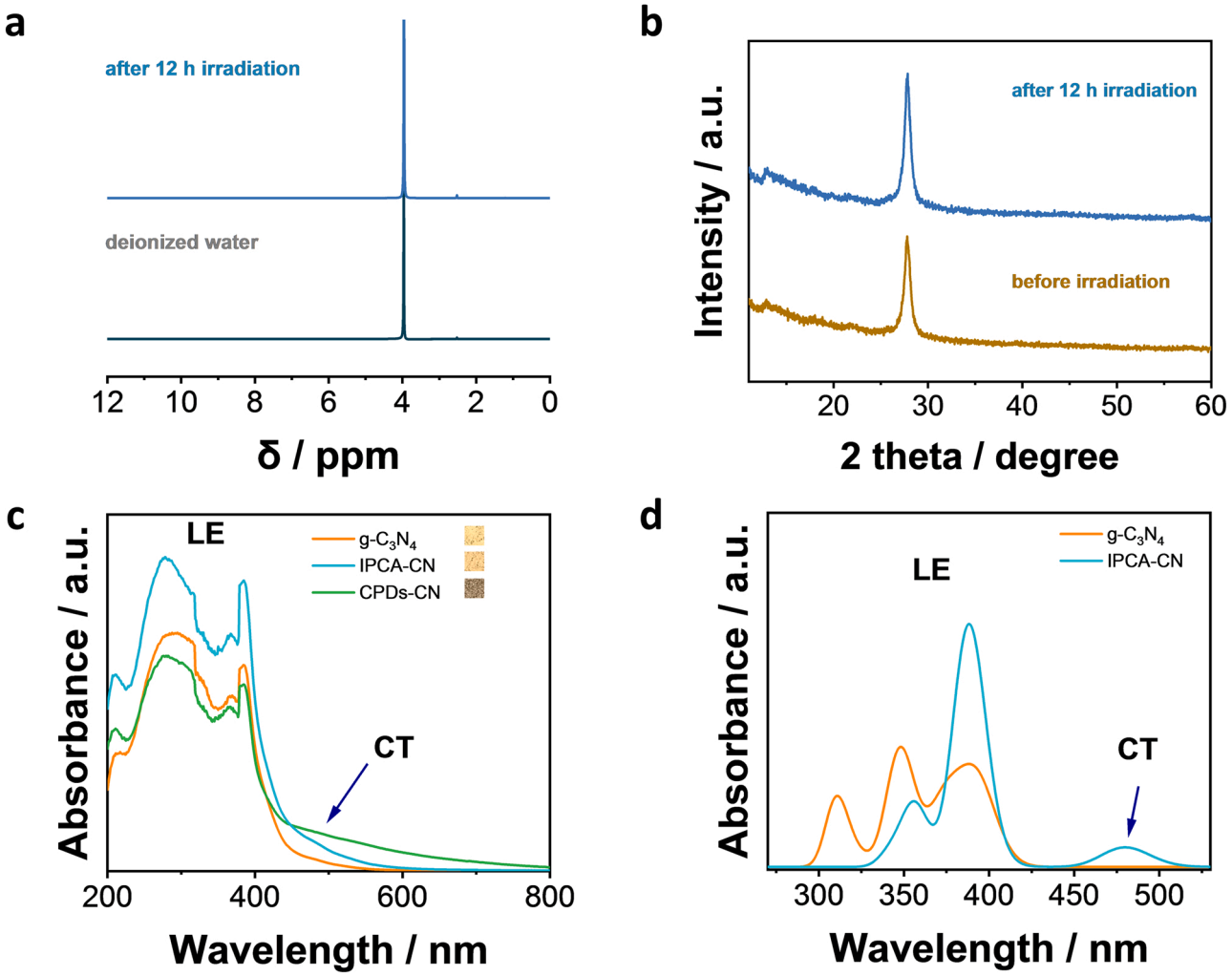

Fig. 2. a) ^{1}H NMR spectra of liquid product before and after 12 h of irradiation over CPDs-CN catalyst. b) XRD patterns of CPDs-CN catalyst before and after 12 h of irradiation. c) UV–vis diffuse reflectance spectra of g-C_3N_4, IPCA-CN and CPDs-CN. Insets: digital photographs of the corresponding samples. d) Calculated absorbance from Gaussian calculations of g-C_3N_4 and IPCA-CN.

fringes of 2.1 Å allow the assignments of the (100) intralayer spacings. In the UV-Vis spectra (Fig. S3), the peaks focused on 240 and 340 nm were assigned to the intrinsic absorption bands originating from the $\pi \rightarrow \pi^*$ electron transition of the sp^2 hybridization conjugated aromatic rings (C═C); new absorption bands were ascribed to the $n \rightarrow \pi^*$ electron transition of the lone pair electrons (C═O), respectively [43]. XPS spectrum suggests that CPDs consist of graphitic sp^2 cores (C═C) and C–N moieties, decorated with hydroxyl (C–OH) and carboxylate functionalities (C═O), providing them with good solubility in water (Fig. S4) [44].

To prove the efficient combination of g-C_3N_4 with CPDs, TEM and XPS were performed. The TEM result of g-C_3N_4 was a two-dimensional layered structure (Fig. S5). In contrast, experimental data indicated that CPDs with ~1·6nm diameters were anchored on the surface of g-C_3N_4 after the hydrothermal treatment (Fig. S6). Compared with g-C_3N_4 (Fig. S7), C 1s spectra were deconvoluted into four peaks for CPDs-CN-3. The peak at 287.1 eV was originated from C═O groups (Fig. S8 and Table S2). Another peak at 397.8 eV in N 1s spectra (Fig. S8 and Table S3) was assigned to amide groups (N–C═O). Furthermore, the O 1s can be matched to N–C═O, C–OH and O_{ads}, while the fitting peak ascribed to carboxyl groups disappeared (Fig. S8 and Table S4). Similarly, XPS spectrum of IPCA-CN was performed, and the carboxyl groups were proved to be nonexistent (Fig. S9 and Tables S2–S4). The presence of carboxyl groups in CPDs-CN-7 proved that these were the remaining groups of the reaction (Fig. S10 and Tables S2-S4). Based on the reaction of carboxyl group and amino group, the carboxyl group from CPDs or IPCA can react with the amino group from g-C_3N_4. The results revealed that the composites were incorporated with g-C_3N_4 by chemical amide bonds [45].

3.3. The mechanism of the photocatalytic reaction

Additionally, the CPDs-CN complex displayed a broad and largely featureless absorption across the near-UV tailing into the visible region above 800 nm according to UV–vis diffuse reflectance spectra (Fig. 2c) [16]. Thus, the incorporation of CPDs may extend the spectral responsive range and deepen color from light yellow to dark brown. In order to explore the mechanism of broadening absorption spectrum by the introduction of CPDs, the structure characteristics of CPDs were carefully studied. First, we noticed that the molecule IPCA on the surface of CPDs considerably contributes to the light absorbance in CPDs (Fig. S3) [46]. Thus, we assume that the broadening of absorption originates from the surface molecule IPCA. To confirm the effect of IPCA on the spectrum broadening, a comparative experiment with IPCA-CN was conducted. The as-prepared IPCA-CN shows a similar absorption band which greatly confirms our assumption (Fig. 2c). To further prove this assumption, we constructed the model systems of g-C_3N_4 and IPCA-CN (Fig. 1a) and the DFT calculations on the UV–vis spectra were carried out for comparison (Fig. 2d and Fig. S11). The results reveal that both g-C_3N_4 and IPCA-CN showed a large absorption band at ~ 300–430 nm

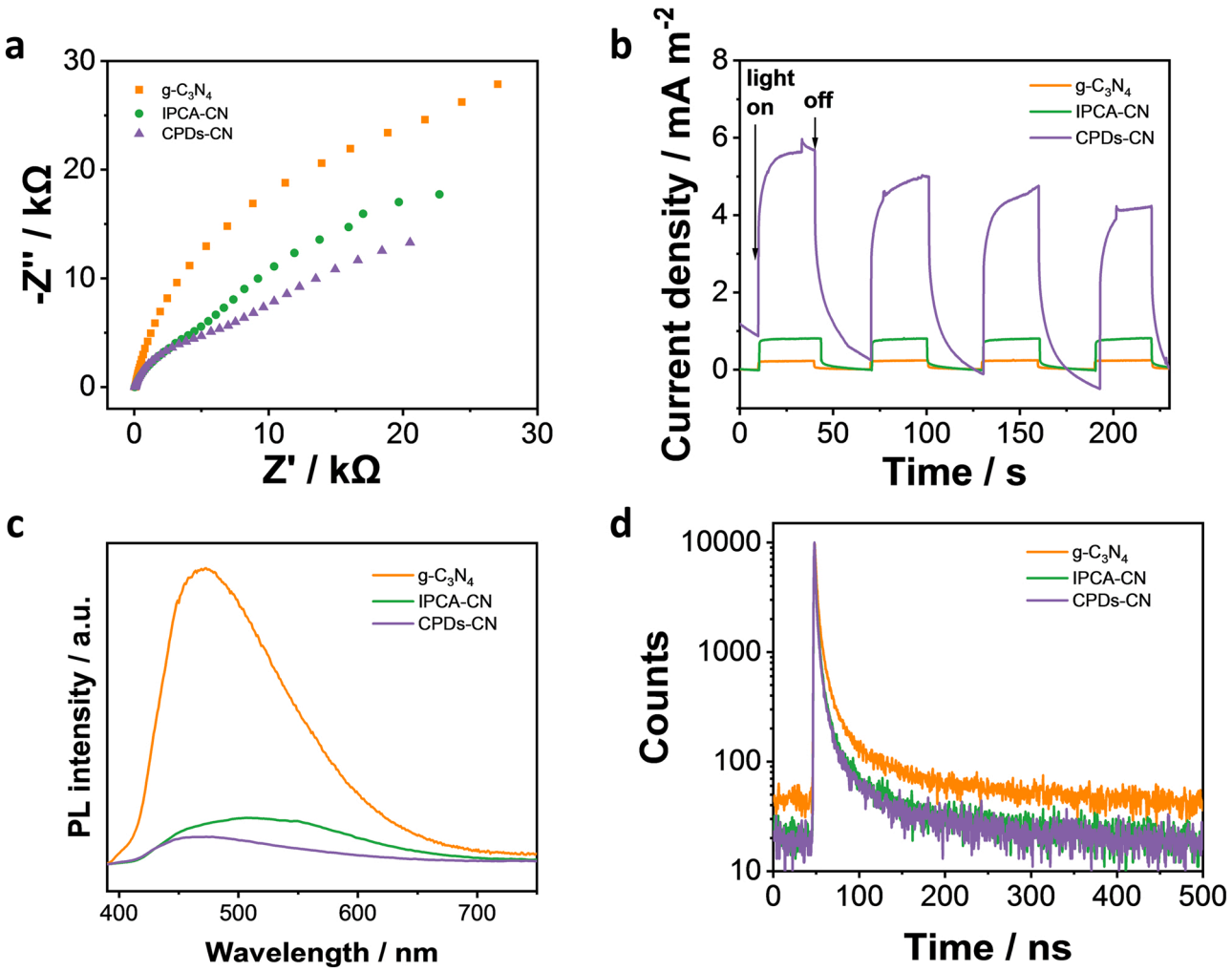

Fig. 3. a) The EIS Nyquist plots. b) The photocurrent–time dependence under chopped illumination with 30 s light on/off cycles. Steady-state fluorescence spectra (c) and fluorescence decay curves (d) of as-prepared samples.

corresponding to the g-C_3N_4 local excitation (LE) (Fig. 2d and Fig. S11), which is in consistent with experimental observation (Fig. 2c). In IPCA-CN, a new absorption peak was observed at around 480 nm in comparison with g-C_3N_4 and the natural transition orbitals (NTO) analysis suggested that the origin of this new peak was characterized as the charge transfer (CT) from IPCA to g-C_3N_4 (Fig. S12). This is in well agreement with the observed broadening absorption band at around 410–600 nm in CPDs-CN and IPCA-CN.

Furthermore, efficient charge separation and transfer are necessary for photocatalytic reactions [47–49]. The electron chemical impedance spectroscopy (EIS) technique was used to probe the charge-transfer properties of the catalysts. EIS spectra show that CPDs-CN and IPCA-CN possess a smaller semicircle radius than g-C_3N_4 (Fig. 3a), indicating that a lower charge-transfer resistance in the composites, which ensures the faster transfer of carriers [11]. Time-dependent photo-response curves of these samples were tested with intermittent irradiation. In Fig. 3b, the photocurrent density of CPDs-CN and IPCA-CN is higher than that of g-C_3N_4, strongly suggesting superior charge generation property compared to g-C_3N_4. Photoluminescence (PL) was employed to further study the recombination abilities of photoexcited electron-hole pairs. A low PL intensity revealed the lower photoinduced charge carriers' recombination. As shown in Fig. 3c, the PL emission intensity of CPDs-CN was the lowest among all the samples with an excitation wavelength at 365 nm, which indicating that the recombination of photogenerated charge carriers was inhibited in the IPCA-CN and CPDs-CN composites. Fig. 3d showed the fluorescence decay curves of as-prepared samples. The calculated average lifetime values of g-C_3N_4, IPCA-CN and CPDs-CN were 21.8, 15.9 and 13.5 ns, respectively. The conclusions suggested that the introduction of IPCA and CPDs retarded the carriers recombination and enhanced the possibility of charge carriers participating in photocatalytic water splitting. Synchronous-illumination X-ray photoelectron spectroscopy was used to directly study the photoinduced charge separation and transfer pathways of CPDs-CN [50,51]. Synchronous light irradiation identical to that used for photocatalytic reactions did not evidently shift O 1s peaks (Fig. S13), but shifted the positions of triazine ring in C 1s and N 1s peaks (by –0.1 and 0.2 eV, respectively, Fig. 4a,b). This result confirmed an increase in the electron density on the N–C═N moieties of triazine rings and the decrease in the electron density on N atoms. These binding energy shifts provided direct evidence of the charge carrier migration pathway. The remarkable properties of CPDs-CN were expected to ameliorate charge separation. As a result, the redistribution of e^- and h^+ markedly minimized their energy-wasteful recombination and enhanced the photoactivity.

The Mulliken charges of the selected atoms in the considered models of g-C_3N_4 and IPCA-CN were calculated and listed (Figs. S14–15, Tables S5–6). The results indicate that the incorporation of IPCA can tune the charges of its chemically bonded 3-s-triazine unit in g-C_3N_4 through amide linkage, effectively, which makes g-C_3N_4 more negative (–1.857 for g-C_3N_4, –2.025 for IPCA-CN, respectively). Upon the adsorption with H_3O^+, the Mulliken charge analysis was also performed (Figs. S16–17, Tables S7–8). The result reveals that IPCA-CN contributes to decreasing charge of H_3O^+ (0.841 for g-C_3N_4@H_3O^+, 0.196 for IPCA-CN@H_3O^+, respectively), which favors the enhancement of photocatalytic proton reduction to H_2.

The schematic diagrams for the excitation and energy transfer pathways of g-C_3N_4@H_3O^+ and IPCA-CN@H_3O^+ complexes from frontier orbital point of view were showed in Fig. 5a,b. The excitation energies, configurations and oscillator strengths are collected in Table 1 and Table 2. For g-C_3N_4@H_3O^+, the highest occupied Kohn-Sham orbital (HOKS) and the second lowest unoccupied Kohn-Sham orbital (LUKS+1) were located around the g-C_3N_4 region, while the lowest unoccupied Kohn-Sham orbital (LUKS) was belonged to H_3O^+. The computed oscillator strength of LE with the value of 0.0025 was much larger than the value 0.0002 of charge transfer (CT) excitation indicating that the charge transfer (CT) state in g-C_3N_4@H_3O^+ could not be generated directly and the excited state energy transfer (ET) from LE state to CT state was suggested as the favorable pathway for g-C_3N_4@H_3O^+ as shown in Fig. 5a. In IPCA-CN@H_3O^+, (HOKS) and (LUKS) were attributed to IPCA and H_3O^+, respectively, the (HOKS–1) and (LUKS+1) were located on the g-C_3N_4 region. Thus, three CT states were found besides LE state as shown in Table 2. Note that the CT1 state corresponding to the IPCA to g-C_3N_4 charge transfer excitation had the largest oscillator strength of 0.0133 which was much larger than the oscillator strength of 0.0021 for LE state and a new absorption band of 579.54 nm was found in IPCA-CN@H_3O^+. More importantly, the introduction of IPCA into g-C_3N_4 could enhance the electron-hole separation due to the higher orbital energy of IPCA, as a result, the electron density of g-C_3N_4 could be increased by additional electron source from IPCA. It is interesting to note that the oscillator strength of CT2 with the value of 0.0056 was also larger than the LE oscillator strength of 0.0021. This indicates that IPCA could also increase the charge transfer excitation to H_3O^+ in comparison with the pristine g-C_3N_4. Consequently, the favorable electron transfer pathway in IPCA-CN@H_3O^+ could follow the IPCA -> g-C_3N_4 -> H_3O^+ procedure as shown in Fig. 5b, and IPCA could be denoted as an active site to increase the electron density on the surface of g-C_3N_4 as well as H_3O^+ which will improve the catalytic efficiency of H_2 generation. Based on all the results from the theoretical calculations and experimental observations, the introduction of CPDs on the surface of g-C_3N_4 could improve the reduction of H^+ and more

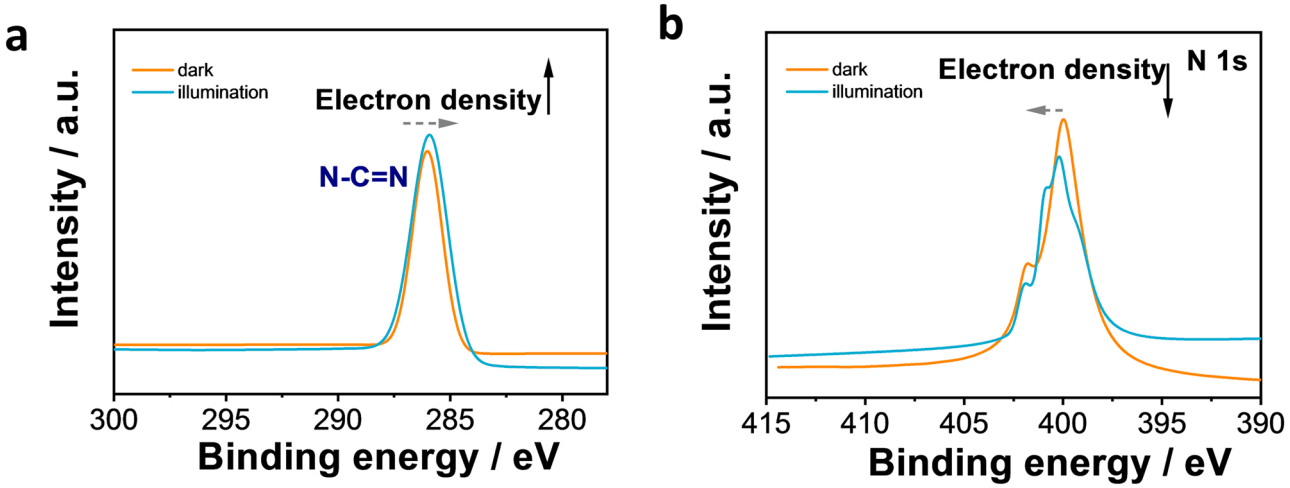

Fig. 4. Synchronous-illumination X-ray photoelectron spectra of (c) N–C═N in the triazine rings and (d) N 1s.

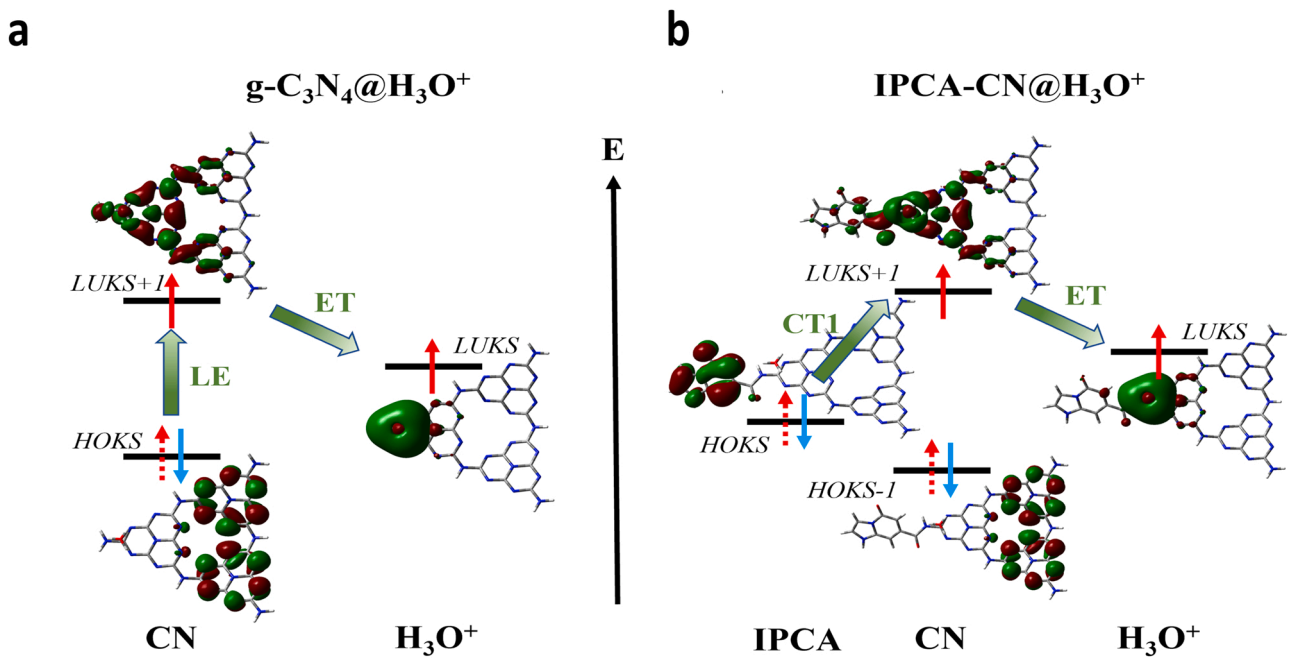

Fig. 5. The schematic diagrams of the energy profile of excitation and energy transfer for (a) g-C_3N_4@H_3O^+ and (b) IPCA-CN@H_3O^+. LE and CT are local excitation and charge transfer excitation, respectively. HOKS and LUKS denote highest occupied Kohn-Sham orbital and lowest unoccupied Kohn-Sham orbital, respectively.

Table 1
The computed excitation energies (ΔE), configurations (Conf.) and oscillator strength (f) of local excitation (LE) and charger transfer (CT) states for g-C_3N_4@H_3O^+ complex.

	LE	CT
ΔE	483.56 nm	775.76 nm
Conf.	$(HOKS)^1 \rightarrow (LUKS+1)^1$	$(HOKS)^1 \rightarrow (LUKS)^1$
f	0.0025	0.0002

Table 2
The computed excitation energies (ΔE), configurations (Conf.) and oscillator strength (f) of local excitation (LE) and charger transfer (CT) states for IPCA-CN@H_3O^+ complex.

	LE	CT1	CT2	CT3
ΔE	506.97 nm	579.54 nm	735.84 nm	1023.46 nm
Conf.	$(HOKS+1)^1 \rightarrow (LUKS+1)^1$	$(HOKS)^1 \rightarrow (LUKS+1)^1$	$(HOKS+1)^1 \rightarrow (LUKS)^1$	$(HOKS)^1 \rightarrow (LUKS)^1$
f	0.0021	0.0133	0.0004	0.0056

conducive to the release of H_2 than g-C_3N_4.

4. Conclusion

In summary, we report the design and synthesis of g-C_3N_4, IPCA-g-C_3N_4 and CPDs-g-C_3N_4 hybrid catalysts. Upon the hybridization with IPCA and CPDs, improved photocatalytic H_2 production rates of g-C_3N_4 were observed (1172 ± 39; 2150 ± 92 vs. 828 ± 121 μmol g^{-1} h^{-1}, respectively). The DFT calculations further unraveled that electron transfer pathway in ICPA-CN@H_3O^+ followed ICPA -> g-C_3N_4 -> H_3O^+ procedure. As a result, we substantially reveal that the surface molecule IPCA of CPDs essentially enhanced the catalytic activity for solar-driven H_2 production in a CPDs-CN system. Molecular IPCA is conducive to extending the light-responsive range and redistributing of photo-induced electron-hole pairs and thus markedly minimizes the energy-wasteful recombination for enhanced photoactivity. This study offers novel insights in utilizing surface molecule to investigate the role of CPDs and how the structure of CPDs contributing to the photocatalytic efficiency, and opens a new avenue towards the design of next generation photocatalysts in future development.

CRediT authorship contribution statement

Mei Han: Conceptualization, Methodology, Software, Formal analysis, Investigation, Writing – original draft, Data curation. **Chunyuan Kang:** Software, Writing – original draft, Data curation. **Zexing Qu:** Conceptualization, Software, Formal analysis, Writing – review & editing, Funding acquisition. **Shoujun Zhu:** Conceptualization, Writing – review & editing. **Bai Yang:** Writing – review & editing, Supervision, Project administration, Funding acquisition.

Declaration of Competing Interest

The authors declare that they have no known competing financial interests or personal relationships that could have appeared to influence the work reported in this paper.

Acknowledgements

This work is supported financially by the National Science Foundation of China (NO. 22035001 and NO. 21873036), JLU Science and Technology Innovative Research Team (2017TD-06) and the GHfund B (20210702).

Appendix A. Supporting information

Supplementary data associated with this article can be found in the online version at doi:10.1016/j.apcatb.2022.121064.

References

[1] Y. Tachibana, L. Vayssieres, J.R. Durrant, Artificial photosynthesis for solar water-splitting, Nat. Photonics 6 (2012) 511–518.
[2] W. Tu, Y. Zhou, Z. Zou, Photocatalytic conversion of CO(2) into renewable hydrocarbon fuels: state-of-the-art accomplishment, challenges, and prospects, Adv. Mater. 26 (2014) 4607–4626.

[3] M.A. Gross, A. Reynal, J.R. Durrant, E. Reisner, Versatile photocatalytic systems for H2 generation in water based on an efficient DuBois-type nickel catalyst, J. Am. Chem. Soc. 136 (2014) 356–366.

[4] A. Indra, A. Acharjya, P.W. Menezes, C. Merschjann, D. Hollmann, M. Schwarze, M. Aktas, A. Friedrich, S. Lochbrunner, A. Thomas, M. Driess, Boosting visible-light-driven photocatalytic hydrogen evolution with an integrated nickel phosphide-carbon nitride system, Angew. Chem. Int. Ed. Engl. 56 (2017) 1653–1657.

[5] F. Pellegrino, F. Sordello, L. Mino, C. Minero, V.-D. Hodoroaba, G. Martra, V. Maurino, Formic acid photoreforming for hydrogen production on shape-controlled anatase TiO2 nanoparticles: assessment of the role of fluorides, {101}/{001} surfaces ratio, and platinization, ACS Catal. 9 (2019) 6692–6697.

[6] T. Hisatomi, K. Domen, Reaction systems for solar hydrogen production via water splitting with particulate semiconductor photocatalysts, Nat. Catal. 2 (2019) 387–399.

[7] A. Agosti, Y. Nakibli, L. Amirav, G. Bergamini, Photosynthetic H2 generation and organic transformations with CdSe@CdS-Pt nanorods for highly efficient solar-to-chemical energy conversion, Nano Energy 70 (2020), 104510.

[8] B.Q. Xia, Y.Z. Zhang, B.Y. Shi, J.R. Ran, K. Davey, S.Z. Qiao, Photocatalysts for hydrogen evolution coupled with production of value-added chemicals, Small Methods 4 (2020).

[9] F. Li, Y. Wang, J. Du, Y. Zhu, C. Xu, L. Sun, Simultaneous oxidation of alcohols and hydrogen evolution in a hybrid system under visible light irradiation, Appl. Catal. B: Environ. 225 (2018) 258–263.

[10] D.S. Achilleos, W. Yang, H. Kasap, A. Savateev, Y. Markushyna, J.R. Durrant, E. Reisner, Solar reforming of biomass with homogeneous carbon dots, Angew. Chem. Int. Ed. 59 (2020) 18184–18188.

[11] C. Kranz, M. Wachtler, Characterizing photocatalysts for water splitting: from atoms to bulk and from slow to ultrafast processes, Chem. Soc. Rev. (2020).

[12] T. Feng, S. Tao, D. Yue, Q. Zeng, W. Chen, B. Yang, Recent advances in energy conversion applications of carbon dots: from optoelectronic devices to electrocatalysis, Small 16 (2020), e2001295.

[13] S. Zhu, J. Zhang, S. Tang, C. Qiao, L. Wang, H. Wang, X. Liu, B. Li, Y. Li, W. Yu, X. Wang, H. Sun, B. Yang, Surface chemistry routes to modulate the photoluminescence of graphene quantum dots: from fluorescence mechanism to up-conversion bioimaging applications, Adv. Funct. Mater. 22 (2012) 4732–4740.

[14] M. Han, S. Zhu, S. Lu, Y. Song, T. Feng, S. Tao, J. Liu, B. Yang, Recent progress on the photocatalysis of carbon dots: classification, mechanism and applications, Nano Today 19 (2018) 201–218.

[15] B.C. Martindale, E. Joliat, C. Bachmann, R. Alberto, E. Reisner, Clean donor oxidation enhances the H2 evolution activity of a carbon quantum dot-molecular catalyst photosystem, Angew. Chem. Int. Ed. Engl. 55 (2016) 9402–9406.

[16] B.C.M. Martindale, G.A.M. Hutton, C.A. Caputo, S. Prantl, R. Godin, J.R. Durrant, E. Reisner, Enhancing light absorption and charge transfer efficiency in carbon dots through graphitization and core nitrogen doping, Angew. Chem. Int. Ed. Engl. 56 (2017) 6459–6463.

[17] C. Xia, S. Zhu, T. Feng, M. Yang, B. Yang, Evolution and synthesis of carbon dots: from carbon dots to carbonized polymer dots, Adv. Sci. 6 (2019), 1901316.

[18] J.J. Liu, Y.J. Geng, D.W. Li, H. Yao, Z.P. Huo, Y.F. Li, K. Zhang, S.J. Zhu, H.T. Wei, W.Q. Xu, J.L. Jiang, B. Yang, Deep red emissive carbonized polymer dots with unprecedented narrow full width at half maximum, Adv. Mater. 32 (2020).

[19] J. Liu, R. Li, B. Yang, Carbon dots: a new type of carbon-based nanomaterial with wide applications, ACS Cent. Sci. 6 (2020) 2179–2195.

[20] Y. Zhang, Y. Zhao, Z. Xu, H. Su, X. Bian, S. Zhang, X. Dong, L. Zeng, T. Zeng, M. Feng, L. Li, V.K. Sharma, Carbon quantum dots implanted CdS nanosheets: efficient visible-light-driven photocatalytic reduction of Cr(VI) under saline conditions, Appl. Catal. B: Environ. 262 (2020), 118306.

[21] X. Chen, J. Wang, Y. Chai, Z. Zhang, Y. Zhu, Efficient photocatalytic overall water splitting induced by the giant internal electric field of a g-C3 N4 /rGO/PDIP Z-scheme heterojunction, Adv. Mater. (2021), e2007479.

[22] W. Jiang, X. Zong, L. An, S. Hua, X. Miao, S. Luan, Y. Wen, F.F. Tao, Z. Sun, Consciously constructing heterojunction or direct Z-scheme photocatalysts by regulating electron flow direction, ACS Catal. 8 (2018) 2209–2217.

[23] X. Li, B. Kang, F. Dong, Z. Zhang, X. Luo, L. Han, J. Huang, Z. Feng, Z. Chen, J. Xu, B. Peng, Z.L. Wang, Enhanced photocatalytic degradation and H2/H2O2 production performance of S-pCN/WO2.72 S-scheme heterojunction with appropriate surface oxygen vacancies, Nano Energy 81 (2021), 105671.

[24] C.A. Caputo, M.A. Gross, V.W. Lau, C. Cavazza, B.V. Lotsch, E. Reisner, Photocatalytic hydrogen production using polymeric carbon nitride with a hydrogenase and a bioinspired synthetic Ni catalyst, Angew. Chem. Int. Ed. Engl. 53 (2014) 11538–11542.

[25] X. Zhao, Y. You, S. Huang, Y. Wu, Y. Ma, G. Zhang, Z. Zhang, Z-scheme photocatalytic production of hydrogen peroxide over Bi4O5Br2/g-C3N4 heterostructure under visible light, Appl. Catal. B: Environ. 278 (2020), 119251.

[26] Y. Zhao, Y. Liu, J. Cao, H. Wang, M. Shao, H. Huang, Y. Liu, Z. Kang, Efficient production of H2O2 via two-channel pathway over ZIF-8/C3N4 composite photocatalyst without any sacrificial agent, Appl. Catal. B: Environ. 278 (2020), 119289.

[27] Y. Shiraishi, Y. Ueda, A. Soramoto, S. Hinokuma, T. Hirai, Photocatalytic hydrogen peroxide splitting on metal-free powders assisted by phosphoric acid as a stabilizer, Nat. Commun. 11 (2020).

[28] F. Wang, Y. Wang, Y. Wu, D. Wei, L. Li, Q. Zhang, H. Liu, Y. Liu, W. Lv, G. Liu, Template-free synthesis of oxygen-containing ultrathin porous carbon quantum dots/g-C3N4 with superior photocatalytic activity for PPCPs remediation, Environ. Sci.: Nano 6 (2019) 2565–2576.

[29] Y. Wang, X. Liu, X. Han, R. Godin, J. Chen, W. Zhou, C. Jiang, J.F. Thompson, K. B. Mustafa, S.A. Shevlin, J.R. Durrant, Z. Guo, J. Tang, Unique hole-accepting carbon-dots promoting selective carbon dioxide reduction nearly 100% to methanol by pure water, Nat. Commun. 11 (2020) 2531.

[30] Y. Song, S. Zhu, S. Zhang, Y. Fu, L. Wang, X. Zhao, B. Yang, Investigation from chemical structure to photoluminescent mechanism: a type of carbon dots from the pyrolysis of citric acid and an amine, J. Mater. Chem. C 3 (2015) 5976–5984.

[31] D. Qu, Z. Sun, The formation mechanism and fluorophores of carbon dots synthesized via a bottom-up route, Mater. Chem. Front. 4 (2020) 400–420.

[32] N. Dhenadhayalan, K.-C. Lin, R. Suresh, P. Ramamurthy, Unravelling the multiple emissive states in citric-acid-derived carbon dots, J. Phys. Chem. C 120 (2016) 1252–1261.

[33] S. Cailotto, R. Mazzaro, F. Enrichi, A. Vomiero, M. Selva, E. Cattaruzza, D. Cristofori, E. Amadio, A. Perosa, Design of carbon dots for metal-free photoredox catalysis, ACS Appl. Mater. Interfaces 10 (2018) 40560–40567.

[34] Q. Fang, Y. Dong, Y. Chen, C.-H. Lu, Y. Chi, H.-H. Yang, T. Yu, Luminescence origin of carbon based dots obtained from citric acid and amino group-containing molecules, Carbon 118 (2017) 319–326.

[35] S. Zhu, Q. Meng, L. Wang, J. Zhang, Y. Song, H. Jin, K. Zhang, H. Sun, H. Wang, B. Yang, Highly photoluminescent carbon dots for multicolor patterning, sensors, and bioimaging, Angew. Chem. Int. Ed. Engl. 52 (2013) 3953–3957.

[36] M. Han, S. Lu, F. Qi, S. Zhu, H. Sun, B. Yang, Carbon dots–implanted graphitic carbon nitride nanosheets for photocatalysis: simultaneously manipulating carrier transport in inter- and intralayers, Sol. RRL 4 (2020), 1900517.

[37] Gaussian16, Revision A.03, M. J. Frisch et al., Gaussian, Inc., Wallingford CT, 2016.

[38] K. Raghavachari, Perspective on “density functional thermochemistry. III. The role of exact exchange” - Becke AD (1993) J Chem Phys 98:5648-52, Theor. Chem. Acc. 103 (2000) 361–363.

[39] A.D. Becke, A new mixing of Hartree–Fock and local density-functional theories, J. Chem. Phys. 98 (1993) 1372–1377.

[40] R.D.W.J. Hehre, J.A. Pople, Self-consistent molecular orbital methods. XII. Further extensions of gaussian-type basis sets for use in molecular orbital studies of organic molecules, J. Chem. Phys. 56 (1972).

[41] X. Jiao, K. Zheng, Q. Chen, X. Li, Y. Li, W. Shao, J. Xu, J. Zhu, Y. Pan, Y. Sun, Y. Xie, Photocatalytic conversion of waste plastics into C2 fuels under simulated natural environment conditions, Angew. Chem. Int. Ed. (2020).

[42] C. Xia, S. Tao, S. Zhu, Y. Song, T. Feng, Q. Zeng, J. Liu, B. Yang, Hydrothermal addition polymerization for ultrahigh-yield carbonized polymer dots with room temperature phosphorescence via nanocomposite, Chemistry 24 (2018) 11303–11308.

[43] S. Mondal, A. Yucknovsky, K. Akulov, N. Ghorai, T. Schwartz, H.N. Ghosh, N. Amdursky, Efficient photosensitizing capabilities and ultrafast carrier dynamics of doped carbon dots, J. Am. Chem. Soc. 141 (2019) 15413–15422.

[44] S. Zhu, J. Zhang, L. Wang, Y. Song, G. Zhang, H. Wang, B. Yang, A general route to make non-conjugated linear polymers luminescent, Chem. Commun. 48 (2012) 10889–10891.

[45] D. Qu, J. Liu, X. Miao, M. Han, H. Zhang, Z. Cui, S. Sun, Z. Kang, H. Fan, Z. Sun, Peering into water splitting mechanism of g-C3N4-carbon dots metal-free photocatalyst, Appl. Catal. B: Environ. 227 (2018) 418–424.

[46] S. Zhu, X. Zhao, Y. Song, S. Lu, B. Yang, Beyond bottom-up carbon nanodots: Citric-acid derived organic molecules, Nano Today 11 (2016) 128–132.

[47] W. Jiang, Y. Zhao, X. Zong, H. Nie, L. Niu, L. An, D. Qu, X. Wang, Z. Kang, Z. Sun, Photocatalyst for high-performance H2 production:ga-doped polymeric carbon nitride, Angew. Chem. Int. Ed. Engl. (2021).

[48] X. Zeng, Y. Liu, Y. Kang, Q. Li, Y. Xia, Y. Zhu, H. Hou, M.H. Uddin, T. R. Gengenbach, D. Xia, C. Sun, D.T. McCarthy, A. Deletic, J. Yu, X. Zhang, Simultaneously tuning charge separation and oxygen reduction pathway on graphitic carbon nitride by polyethylenimine for boosted photocatalytic hydrogen peroxide production, ACS Catal. 10 (2020) 3697–3706.

[49] C.M. Wolff, P.D. Frischmann, M. Schulze, B.J. Bohn, R. Wein, P. Livadas, M. T. Carlson, F. Jäckel, J. Feldmann, F. Würthner, J.K. Stolarczyk, All-in-one visible-light-driven water splitting by combining nanoparticulate and molecular co-catalysts on CdS nanorods, Nat. Energy 3 (2018) 862–869.

[50] X. Liu, G. Dong, S. Li, G. Lu, Y. Bi, Direct observation of charge separation on anatase TiO2 crystals with selectively etched {001} facets, J. Am. Chem. Soc. 138 (2016) 2917–2920.

[51] J. Low, B. Dai, T. Tong, C. Jiang, J. Yu, In situ irradiated X-Ray photoelectron spectroscopy investigation on a direct Z-scheme TiO2/CdS composite film photocatalyst, Adv. Mater. 31 (2019), 1802981.